

**INTERANNUAL LENGTH-OF-DAY VARIATIONS AND THE ENSO  
PHENOMENON: INSIGHTS VIA SINGULAR SPECTRA]. ANALYSIS**

by

J. O. Dickey and C.L. Keppenne<sup>1</sup>

Space Geodetic Science and Applications Group  
Jet Propulsion Laboratory  
California Institute of Technology  
Pasadena, California 91109-8099 USA

<sup>1</sup>Now at High Performance and Concurrence Computing, Pasadena

*J. Geophys. Res.* (submitted)

September 24, 1997

## **Table of Contents**

Abstract

1. Introduction
2. Description of Data
  - Length-of-Day
  - Southern Oscillation Index
3. Analysis Technique
  - Singular Spectrum Analysis
  - Maximum Entropy: Spectral Estimation
4. Analysis and Interpretation
5. Concluding Remarks

Acknowledgments

References

Figure Captions

Figures

## Abstract

Singular spectrum analysis (SSA), used in both single channel and complex SSA (CSSA) modes, is applied to time series of Length-of-Day (LOD) variations and the Modified Southern Oscillation Index (MSOI), focusing on interannual periods. A robust quasi-biennial (QB) oscillation is observed at -28 months, with strong low frequency (LF) components seen at -54 months, in both series for the period 1962–1996. The restructured series from separate channel SSA analyses are closely related, with maximum correlation coefficients of 0.87, 0.82, and 0.90 for the QB, LF and full El Niño/Southern Oscillation (ENSO) bands, respectively, and with complex SSA showing a slightly higher correlation of 0.93 for the full ENSO variability. ENSO events occur when both the QB and LF components add constructively, with positive LOD and MSOI anomalies indicative of an El Niño (warm event—in which an increase in atmospheric angular momentum results in high LOD values), while a decrease in LOD and MSOI reflects cold (La Niña) events. No discernible lags or leads between the two series are observed. ‘It is the sum of these components, LF plus QB—the full ENSO variability—that is the most coherent, indicating the robust link between the ENSO phenomena and interannual LOD variations. The correlation, the largest reported to date, confirms the success of SSA in separating signal from background noise. Decadal variability is also observed in both series.

### *1. Introduction*

The rotation rate of the solid Earth exhibits minute but complicated changes of up to several parts in  $10^8$  in speed [corresponding to a variation of several milliseconds in the length of day (LOD)—Fig. 1] and even larger variations in the direction of the rotation axis (polar motion). These changes occur over a broad spectrum of time scales, ranging from days to centuries and longer, reflecting the fact that they are produced by a wide variety of geophysical and astronomical phenomena (see for example, *Lambeck, 1988; Hide and Dickey, 1991; Rosen, 1993*). Changes in LOD at seasonal and higher frequencies can be

attributed primarily to exchange of angular momentum with the atmosphere, with zonal frictional stress and surface pressure gradients acting as agents for transferring angular momentum between the atmosphere and the Earth. At the other end of the frequency domain, tidal dissipation, post-glacial rebound and core-mantle interactions are accepted as the causes of the long-term (secular to decade) variations in LOD. Intermediate between these regimes are the interannual variations ( $\Lambda_\beta$  using the notation of *Hide and Dickey*, 1991) which are dominated by atmospheric effects, with some indication of an oceanic contribution [*Dickey et al.*, 1993 and 1994].

Several earlier studies have attempted to link  $\Lambda_\beta$  to the Quasi-Biennial Oscillation (QBO) [for a review, see *Lambeck*, Chapter 7, 1980]. Initially, *Lambeck and Cazenave* [1973] associated  $\Lambda_\beta$  changes during the 1955-71 period with the QBO. Later, *Stephancic* [1982] proposed a connection between  $\Lambda_\beta$  and the Southern Oscillation by establishing coherence between  $\Lambda_\beta$  and equatorial Pacific air temperature (whose fluctuation is a good index of the Southern Oscillation phenomenon). He speculated that the coherence was caused by zonal wind anomalies originating in the tropics. Further investigations were stimulated by the occurrence of the unusually strong and well observed El Niño of 1982-83 [see e.g., *Philander*, 1983 and 1990; *Rasmusson and Wallace*, 1983]. The largest changes ever recorded in LOD and  $\Lambda_\beta$  occurred during January and February 1983 [*Rosen et al.*, 1984 and *Eubanks et al.*, 1985].

The El Niño/Southern Oscillation (ENSO) phenomenon is associated with persistent but irregular variations of atmospheric pressure over the tropical Pacific on interannual time scales. This gives rise to pronounced year-to-year variations in the climate of the Pacific basin [*Rasmusson and Wallace*, 1983] associated with extensive fluctuations in the atmospheric and oceanic circulation and in sea surface temperatures [*Philander*, 1983, 1990]. The dynamical processes involved include nonlinear air-sea interactions, with changes in the sea surface temperature causing changes in the surface winds which, in turn, modify ocean surface waters, providing a feedback loop. The persistence of the oscillation

is probably a consequence of the thermal inertia of the oceans, which provides a means of storing heat from one year to the next. According to a model by *Wyrtki [1985]*, the ENSO cycle is driven by the steady accumulation of warm water in the western part of the equatorial Pacific caused by the prevailing surface easterly winds. An El Niño event is triggered by a relaxation of the easterlies, which causes a surge of warm water to move from the west to the east Pacific until it encounters the coasts of North and South America, where it is deflected to higher latitudes in both hemispheres. The El Niño events thus serve to remove the excess warm equatorial water, setting the stage for the oscillation to begin again. The associated “Southern Oscillation” in surface air pressure has the structure of a standing wave, with antinodes near the eastern and western boundaries of the South Pacific,  $-90^\circ$  longitude apart [*Horel and Wallace, 1981*]. This has led to the development of various Southern Oscillation indices (SOI) based on the difference between sea level surface pressure in the east and west Pacific. The most commonly used index is based on the normalized seasonally adjusted pressure difference between Tahiti, in the east, and Darwin, Australia, in the west [*Chen, 1982*].

Comparisons between  $\Lambda_\beta$  and the strength of the ENSO cycle, represented by the Southern Oscillation Index (SOI or MSOI—see following section) series, have indicated striking agreement [*Chao, 1984, 1988, 1989; Eubanks, 1986; Salstein and Rosen, 1986; Gambis, 1992; and Dickey et al., 1993 and 1994*], with high interannual values of LOD generally coinciding with ENSO events. During an ENSO event, the MSOI (SOI) reaches a maximum (minimum), leading to an increase in atmospheric angular momentum (AAM) associated with the collapse of the tropical easterlies. Further increases in AAM may result from a strengthening of westerly flow in the subtropical jet streams [*Rosen et al., 1984*]. Conservation of total angular momentum then requires the Earth’s rate of rotation to slow down, thus increasing LOD. Significant correlation exists back to 1930 [*Dickey et al., 1993 and Jordi et al., 1994*], with currently available historical LOD series being unable to resolve interannual signals before this time.

In this study, we utilize the technique of singular spectrum analysis (SSA) in both a single-channel and multi-channel mode to explore the relationship between Earth rotation and ENSO phenomena on interannual time scales. A description of the data sets is presented in Section 2. The SSA and Maximum Entropy Method (MEM) techniques are described in Section 3, with the analysis and interpretation featured in Section 4. The final section provides a discussion and a summary.

## *2. Description of the Data*

### *2.1 Length-of-Day*

The LOD series utilized (Figure 1) is the Jet Propulsion Laboratory (JPL) Kalman-filtered series, designated as COMB95 [Gross, 1996; Gross *et al.*, 1997], which is derived from a Kalman filter-based combination of independent Earth rotation measurements utilizing the techniques of optical astrometry, very long baseline interferometry (VLBI) and lunar laser ranging (LLR) to form a high-quality series. Issues of reference frame commonality and the unevenness of data quality and quantity have been addressed and tidal effects have been removed. The LOD series spans the period January 20.0, 1962 through January 17, 1996 at 5 day intervals.

### *2.2 Southern Oscillation Index*

We use here a modified version of the index based on the Tahiti and Darwin sea level pressure (SLP) data, provided by the National Center for Environmental Prediction [K. Mo, personal communication]. The time series is obtained here by first removing the annual cycle (this is done by subtracting from both time series the mean SLP value at that location for the corresponding month), dividing the monthly anomalies so obtained by the corresponding standard deviation, and then taking the Darwin-minus-Tahiti differences. Note the series used here, the “Modified Southern Oscillation Index” (MSOI), is opposite

in sign than that which is commonly used [e. g., *Trenberth and Shea*, 1987], so as to be positively correlated with the LOD (see Fig. 4).

### 3. Analysis Technique

#### 3.1 Singular Spectrum Analysis (SSA)

SSA is the term used in a number of recent climate studies [e.g., *Vautard and Ghil*, 1989; *Rasmusson et al.*, 1990; *Ghil and Vautard*, 1991] to refer to the univariate application of principal component analyses (PCA) [e.g., *Preisendorfer*, 1988] in the time domain. The method is also known as Karhunen-Loève (K-L) expansion [e.g., *Pike et al.*, 1984] in digital signal processing. It was introduced into biological oceanography by *Colebrook* [1978], into nonlinear dynamics by *Broomhead and King* [1986], and into paleoclimatology by *Fraedrich* [1986]. *Rasmusson et al.* [1990] also used SSA to investigate the quasi-biennial component of ENSO.

SSA is algorithmically equivalent to the application of extended empirical orthogonal functions (EEOFs) [e.g., *Weare and Nasstrom*, 1982; *Lau and Chan*, 1986; *Graham et al.*, 1987a, b] to a univariate time series but has special features and greater flexibility when applied to the analysis of phenomena with longer time scales and higher sampling rates [*Ghil and Mo*, 1991 a & b and 1992]. *Vautard et al.* [1992] provide a review of SSA and of its applications to data-adaptive filtering and noise reduction. For brevity, we sketch here the method based on its relation to spatial empirical orthogonal function (EOF) analysis [e.g., *Preisendorfer*, 1988], which is of more common use in meteorology.

Spatial EOF (S-EOF) analysis proceeds by expanding the history of a discrete field  $x_{i,j}$ , where the indices  $i$  and  $j$  refer to the spatial and temporal directions respectively— $1 \leq i \leq M, 1 \leq j \leq N$ —into the sets of its eigenvectors (EOFs) and principal components (PCs). In SSA, the spatial direction is replaced by time lags, i.e.,  $x_{i,j} = x_{j+i}$ , and  $M$  becomes the number of lags. The algebraic formulation remains essentially the same but the T-PCs are shorter than the original time series by  $M - 1$  components. *Vautard and Ghil*

[1989] refer to the EOFs and PCS of SSA as T-EOFs and T-PCs to distinguish them from their counterparts in S-EOF analysis.

The time scales of the dynamics addressed by SSA are bounded from below by the sampling interval,  $\tau$ , and from above by the window width,  $\tau_w = M\tau$  [Vautard *et al.*, 1992]. The choice of  $M$  is a trade-off between the amount of information one wishes to retain and the degree of statistical significance that is required. Increasing  $M$  enhances the former at the expense of the latter, and vice versa.

In contrast with standard spectral analysis in which the basis functions are given *a priori* (e.g., the sines and cosines of Fourier analysis), in SSA they are determined from the data themselves to form an orthogonal basis that is optimal in the statistical sense. Oscillatory modes can be identified as pairs of nearly equal eigenvalues, while their eigenfunctions (T-EOFs) and T-PCs have the same time scale of oscillation, as well as being nearly  $90^\circ$  out of phase [Vautard and Ghil, 1989; Vautard *et al.*, 1992]. Because of this property, the method is particularly helpful in isolating enharmonic oscillations with fluctuating amplitudes from noisy data.

The part of the time series' variability corresponding to a given oscillation can be isolated by restricting the K-L expansion to the T-EOFs and T-PCs that have been identified as corresponding to that oscillation [Ghil and Vautard, 1991; Vautard *et al.*, 1992]. The reconstructed components (RCs) which carry the contributions of the individual T-EOFs and T-PCs to the variance of the data are time series of length  $N$  (not  $N - M + 1$ , like the T-PCs). The RCS are additive and their complete sum gives back the original time series.

The eigenvalue associated with a T-EOF gives the variance of the corresponding T-PC, while its square root is the associated singular value (SV). The SVS are standard deviations and give their name to the SSA method.

### 3.2 Maximum Entropy: Spectral Estimation

The main advantage of the maximum entropy method (MEM) [Yule, 1927; Walker, 1931; Burg, 1968] is its high spectral resolution, obtained by fitting relatively high-order AR models to the data. Its main drawback is the possible appearance of spurious peaks as the resolution, and hence the order, of the method is increased [Childers, 1978].

The basic assumption underlying MEM is that the time series can be modeled by an AR process. The optimal order of the AR process for a given time series is usually inferred from Akaike's information criterion (AIC) [Akaike, 1974]. However, the AIC often calls for a very high order if the data have not been prefiltered. SSA can be used to compute a data-adaptive prefilter by retaining only the leading, statistically significant T-PCs of a given time series [Ghil and Vautard, 1991; Vautard et al., 1992]. Removal of the noise by SSA permits the application of a low-order MEM, which achieves the same resolution as a much higher-order one, without the introduction of spurious peaks. This two-step procedure for spectral estimation is discussed in detail and applied to synthetic examples and to time series of atmospheric angular momentum by Penland et al. [1991].

#### 4. Results and Interpretation

SSA is applied to LOD data (Fig. 1) with a window width of  $\tau_w = 60$  months with  $\tau = 1$  month (monthly data) and  $M = 60$ . This allows us to investigate a broad range of time scales while ensuring a high degree of statistical significance. The first 14 SVS (Fig. 2) explain the bulk of variance with remaining SVS being within the noise floor, as evidenced by the break in the slope of the singular spectrum [Vautard and Ghil, 1989].

The first two SVS (SV1 and 2) capture the long-term decadal variability that has been associated with core-mantle coupling. The contribution of SV 1 and 2 peaks (not shown) in the early 1970s and reaches a minimum in 1986 and increases thereafter; together they explain 18% of total variance of the series. The next nearly equal pair (SVS 3 and 4) captures the strong annual cycle with the terms being in quadrature (Fig. 3a) explaining 15% of the total variance, while the nearly equal pair, SVS 5 and 6, corresponds

to the semi-annual cycle, explaining the 10% of variance (Fig. 3b). Their envelopes are not constant in time but are modulated on interannual to secular time scales. In particular, the decadal LOD modulation matches the decadal variability of the ENSO cycle, with maxima (minima) in the semiannual (annual) component occurring roughly at the times the strong ENSO events of 1972 and 1982 (see Fig. 3a and b---note we exclude the beginning and end of this series to avoid end effects). This indicates a linkage between seasonal LOD variability and the ENSO phenomena, which occurs via non-linear interactions [*Gross et al.*, 1997].

The dominant decadal variability (SVS 1 and 2) and seasonal variability (SVS 3-6) was removed from the LOD, resulting in a series that is dominated by interannual variability (denoted as LOD $\dagger$ ) and is well correlated with the MSOI (see Fig. 4). Single-channel SSA was utilized on both the MSOI and LOD $\dagger$  time series separately; in addition, complex SSA (CSSA) was applied jointly to both series (Fig. 5), with the LOD $\dagger$  taken as the real part and MSOI as the imaginary part, with the goal of studying joint variability. For all three analyses (see Fig. 5) the first pair was associated with the low frequency component (4–6 yr period) of ENSO, with the second pair capturing the quasi-biennial oscillation (2–3 yr period). Slightly higher interannual variance was seen in the MSOI as compared with the LOD $\dagger$  series. For example, the LF component of MSOI explains 14% of the variance, whereas the LOD $\dagger$  component accounts for 12.7%. Similarly for the QB component, the corresponding numbers are 12.7% for MSOI and 10.7% for the LOD series. Complex SSA results lie midway between these numbers for the LF component (explaining 13% of variance), while for the QB component, the CSSA results are consistent with the single channel and LOD results. Similar bimodal behavior has been investigated for the Southern Oscillation Index using SSA by *Rasmusson et al.* [1990] and by *Keppenne and Ghil* [1992]; *Jiang et al.* [1992] applied multi-channel SSA to equatorial wind and sea surface temperature. Fourier spectral analysis has also revealed this phenomenon in LOD [*Dickey et al.*, 1992].

The LF, QB, and the full ENSO components of interannual LOD are isolated by summing the contributions of T-PCs 1 and 2, T-PCs 3 and 4, and T-PCs 1-4 respectively, using the reconstruction method justified rigorously by *Vautard et al.* [1992, equation (2. 17)]. Fig. 6 displays the results (solid for LOD and dashed for MSOI) for both single channel (Fig. 6a-c) and multichannel (Fig. 6d-f) SSA for the LF (Figs. 6a, d) and QB (Figs. 6b, e) components and their sum (Figs. 6c and f). The two series track quite well for the single channel analyses (Fig. 6a-c), with excellent agreement seen in the full ENSO amplitude (Fig. 6c). Typically, the CSSA amplitudes are of similar size to the single channel results indicating the robust connection between these analyses. The cold (La Niña) events of 1971, 1974, 1976, and 1988 are seen as minima in both LOD† and MSOI (see Fig. 6c and f), whereas the warm events are observed as maxima in LOD† and MSOI (minor episodes in 1965, 1969, 1977, and 1987 with strong events in 1972 and 1982). Here, the classification of cold and warm events follows that of *Rasmusson and Carpenter [1982]* and *Deser and Wallace [1987]*, which is broadly accepted. Note the complex nature of the 1991-93 warm events, with a double peak occurring in all components. Decadal variability is also evident, with strong cold events in the early and mid- 1970s and in 1988 and robust warm events in the early and mid- 1980s.

High correlation, seen visually in the comparison of the time series, reaches a maximum of 0.87, 0.82, and 0.90 for QB, LF, and full ENSO variability, respectively, with no discernible lag or lead between the two series (Figs. 8a and b). Secondary maxima are also evident—indicative of the relevant periods. It is interesting to note that it is the sum of two components that is the most coherent. The LF component, with the fewest repeat cycles, has the lowest correlation of the three. The CSSA correlation (0.93) is the largest. Past studies have shown the LOD-SOI correlation to be dependent on the time series considered, and the filtering applied to the series. Using a 1-year minus 5-year moving average to isolate interannual variability *Dickey et al.* [1994] obtained a maximum cross correlation of 0.67 for the period 1962–1988 and a correlation of 0.79 for the period 1972-

1986. *Chao* [1984] reported a correlation coefficient of 0.56 for the period 1957-1983, while *Eubanks et al.* [1986] computed a correlation coefficient of -0.5 for the period 1962-84, and *Chao* [1988] found a correlation of 0.68 for the period 1962-84. *Chao* [1989] also obtained a correlation coefficient of 0.75 for the period 1964-84 by using multiple regression on the SOI and a stratospheric AAM series, derived from monthly data from three stations using an idealized model of the QBO. The results of the present study give the largest correlation to date, indicating the success of SSA in separating signal from the background noise, particularly for the full ENSO variability, reconstructed from single channel or complex SSA analyses.

ENSOS generally occur when both the QB and LF components add constructively, with positive MSOI/LOD anomalies indicating a warm (El Niño) event while negative MSOI/LOD reflects a cold (La Niña) event (e.g., *Rasmusson et al.*, 1990, *Keppenne and Ghil*, 1992, and *Dickey et al.*, 1992). Note, for example, the constructive nature of the 1972, 1982-83, and 1986-87 warm events, which result in an El Niño amplitude (Fig. 6c) that is considerably larger than the individual components (Figs. 6a and b—note the difference in scale). Similarly, the coherently-phased negative amplitudes of these components during 1988 produced an intense cold (La Niña) event. Interference between these bands results in the complex nature of the full ENSO series; for example, the QB oscillation with minima in 1974 and 1976 (Fig 6b) adds with single negative peak in LF components (centered in 1975, Fig. 6a) to produce two consecutive cold events in 1974 and 1976. In contrast, destructive interference between these two components in 1980 and 1985 results in a lack of pronounced ENSO variability during these times.

The spectra of the two reconstructed series (Fig. 7) have common bimodal structure, with the low frequency being centered at 53 months in the LOD and at 55 months in the MSOI, while the QB peak is centered at 29 months in LOD, and at 28 months in the MSOI. In the CSSA case, the common periodicity in the LF band is 54 months, while that of the QB is 28 months. The time variation of LOD<sup>†</sup>-MSOI correlations are displayed in

Figs. 9a and 9b, using a window of 60 months for the single channel and complex SSA, respectively. Typically, the full ENSO component is more coherent, with LOD-MSOI correlation of 0.85 or larger for both the single channel SSA and the CSSA cases. The correlation is most variable for the QB component, reaching a minimum of - 0.54 for single channel case in 1968. This is caused by the mismatch of the two series in 1968 (Fig. 6b); in the MSOI, a maximum occurs in 1967, whereas a plateau is seen in the LOD $\dagger$ . The relative minima in the LF component (1971 and 1979—Fig. 9a) are associated with relative phase shifts between LOD $\dagger$  and MSOI (Fig. 6a). The CSSA coherence is higher; a relative dip (ranging from -0.8 to 0.85) is seen in all three components in 1978, and is caused phase differences between the series. It should be noted that the LOD $\dagger$  QB variation reflects the contribution of the whole atmosphere, including the troposphere and the stratosphere, with the latter being a major contributor. During the 1982-83 ENSO event, for example, the stratospheric winds integrated from 100 to 1 mb explained 20% of the interannual LOD variance [Dickey *et al.*, 1994]. The QB oscillation in the MSOI, on the other hand, appears to be a tropospheric phenomenon (e.g. *Xu*, 1992).

## 5. Summary and Discussion

The El Niño/Southern Oscillation (ENSO) phenomenon involves large-scale redistribution of atmospheric mass between the eastern and western ends of the Pacific, and is associated with changes in both atmospheric and oceanic circulation (Philander, 1990). During a warm (El Niño) event the MSOI reaches a maximum, with a concomitant collapse of the tropical easterlies and an increase in global AAM. Conservation of total angular momentum requires the Earth's rate of rotation to diminish, causing LOD to increase. A further increase in AAM may result from the large-scale heating of the tropical troposphere associated with the El Niño events (Stephanick, 1982), leading to a zonally symmetric rise

in the tropical 200 mb height field (Horel and Wallace, 1981) and a consequent strengthening of the upper-level subtropical jet streams.

In this study, we have utilized both complex and single-channel singular spectrum analysis (SSA) to study interannual variations in the Earth's rate of rotation, and hence, in the length of day (LOD), and its link to the ENSO phenomenon, indicated by variations in the Modified Southern Oscillation Index (MSOI), during the period 1962–1996. Our results underscore the pronounced bimodal nature of ENSO, with a strong quasi-biennial (QB) oscillation centered at -28 months and a robust low frequency (LF) component at -53–55 months in both series. The restructured LOD and MSOI signals from separate channel SSA are highly correlated, with maximum of coefficients of 0.87, 0.82, and 0.90 for the QB, LF, and full ENSO band. The application of complex SSA (CSSA with LOD taken as the real and MSOI as the imaginary part) assesses the joint variability of the two series. The CSSA results are similar (Fig. 6), having slightly higher correlation than the single channel findings, and with the sum of LF and QB components having the largest cross-correlation (0.93—see Fig. 8). ENSO events occur when both the LF and QB components add coherently, with positive LOD and MSOI indicative of an increase in atmospheric angular momentum (AAM) during warm (El Niño) events; conversely, a cold (La Niña) event reflects a decrease in AAM and LOD. No discernible lag or lead between the two series, each given at monthly intervals, is observed. The strong LOD-MSOI correlation, the largest reported to date by a significant amount, further confirms the success of SSA in separating signal from background noise in geophysical series, and affirms the causal link between the dynamics of Earth rotation and the ENSO phenomenon.

### *Acknowledgments*

We acknowledged interesting discussions with M. Ghil, S. L. Marcus, and R. Hide. The authors thank K. Mo and E. Rasmussen for supplying SOI data used in our analysis, and S. L. Marcus for helpful suggestions on the manuscript. This paper presents the results of

one phase of research carried out at the Jet Propulsion Laboratory, California Institute of Technology, sponsored by the National Aeronautics and Space Administration (NASA) and National Oceanic and Atmospheric Administration (NOAA).

### *Figure Captions*

Fig. 1a. Monthly length-of-day (LOD) time determinations derived from a Kalman filter-based combination [Gross, 1996] of independent Earth rotation measurements.

Fig. 2. Normalized eigenvalue spectrum of the lag-covariance matrix of the length-of-day time series shown in Fig. 1 with a window size of 60 months. The singular values corresponding to three pairs of oscillations are pointed out, notably long-term trends (1-2), annual (3-4) and semi-annual (5-6) variations.

Fig. 3. The reconstructed LOD time series (in ms) obtained by combining the variance associated with two pairs of temporal principal components (T-PCs) (a) Annual component: Principal components (PCs): PCs 3 and 4; (b) Semi-annual components: PCs 5 and 6.

Fig. 4. (a) Length-of-day time anomaly (LOD $\dagger$ ) series after the removal of the annual and semi-annual components (PC 3-6) and the PCs (1-2) representing the longer term decadal effects and (b) the MSOI time series (Darwin minus Tahiti sea level pressure-see text for details). Note that both series are dimensionless.

Fig. 5. Normalized eigenvalue spectrum of the lag-covariance matrix of the LOD $\dagger$  and MSOI time series as shown in Fig. 4 with a window size of 60 months. Results from both singular channel and complex SSA are displayed. The first pair (SV 1-2) corresponds to

the low frequency ENSO oscillation, while the second corresponds to the quasi-biennial ENSO (3-4) variability.

Fig. 6. Reconstructed  $\text{LOD}^\dagger$  (solid line) and MSOI (dashed line) time series obtained by combining the variance associated with temporal principal components (T-PCs). (a) and (d) display the low frequency component; (b) and (e) the quasi-biennial component; and (c) and (f) is the sum of the two components; (a)--(c) shows the results of single channel SSA, while (d)-(f) are the corresponding complex SSA series.

Fig. 7. Maximum Entropy Method (MEM) power spectra of  $\text{LOD}^\dagger$  (filled circles) and the MSOI (open circles) as obtained from single channel (a) and multi-channel SSA (b).

Fig. 8. (a) Correlation as a function of lag between the Modified Southern Oscillation Index and Length-of-Day ( $\text{LOD}^\dagger$ ) as analyzed by single channel SSA. Both bands (PC 1-4) are indicated by the connected squares (maximum correlation = 0.90); the low frequency (PC 1 and 2) is represented by the connected full circles (maximum correlation = 0.78); and the quasi-biennial band is indicated by the connected open circles (maximum correlation = 0.86); (b) results from complex SSA.

Fig. 9. (a) Correlation as a function time using a window of 60 months for single channel SSA; and (b) same as (a) for multichannel SSA.

## References

- Akaike, H., A new look at the statistical model identification, *IEEE Trans. Autom. Control*, AC-19, 716-723, 1974.
- Broomhead, D. S., and G. P. King, Extracting qualitative dynamics from experimental data, *Phys. D Amsterdam*, 20, 217-236, 1986.
- Burg, J. P., Maximum entropy spectral analysis, in *Modern Spectrum Analysis*, edited by D. G. Childers, pp. 34-48, IEEE Press, New York, 1968.
- Chao, B. F., Interannual length-of-day variations with relation to the Southern Oscillation/El Niño, *Geophys. Res. Lett.*, 11, 541-544, 1984.
- Chao, B. F., Correlation of interannual length-of-day variation with El Niño/Southern Oscillation, 1972-1986, *J. Geophys. Res.*, 93, 7709-7715, 1988.
- Chao, B. F., Length-of-day variations caused by El Niño/Southern Oscillation and the quasi-biennial oscillation, *Science*, 243, 923-925, 1989.
- Childers, D. G. (cd.), *Modern Spectral Analysis*, IEEE Press, New York, 1978.
- Colebrook, J. M., Continuous plankton records: Zooplankton and environment, North-East Atlantic and North Sea, 1948-1975, *Oceanol. Acts*, 1, 9-23, 1978.
- Deser, C., and J. M. Wallace, El Niño events and their relation to the Southern Oscillation: 1925-86, *J. Geophys. Res.*, 92, 14,189-14,196, 1987.
- Dickey, J. O., S. L. Marcus, R. Hide, T. M. Eubanks, and D. H. Boggs, Angular Momentum Exchange Among the Solid Earth, Atmosphere, and Oceans—A Case Study of the 1982-83 El Niño Event, *J. Geophys. Res.*, 99, 23,921-23937, 1994.
- Dickey, J. O., S. L. Marcus, T. M. Eubanks, and R. Hide, Climate studies via space geodesy: Relationships between ENSO and interannual length-of-day variations, in *Interactions Between Global Climate Subsystems: The Legacy of Hann*, *Geophys.*

- Monogr. Ser., vol. 75*, edited by G. A. McBean and M. Hantel, pp. 141-155, AGU, Washington, D. C., 1993.
- Dickey, J. O., S. L. Marcus, and R. Hide, Global Propagation of Interannual Fluctuations in Atmospheric Angular Momentum, *Nature*, 357, 484-488, 1992.
- Eubanks, T. M., J. O. Dickey, and J. A. Steppe, The 1982-83 El Niño, the Southern Oscillation, and changes in the length of day, *Trop. Ocean Atmos. News.*, 29, 21-23, 1985.
- Eubanks, T. M., J. A. Steppe, and J. O. Dickey, The El Niño, the Southern Oscillation and the Earth's Rotation, in *Earth Rotation: Solved and Unsolved Problem, NATO Advanced Institute Series C: Mathematical and Physical Sciences*, 187, ed. A. Cazenave, 163-186, D. Reidel, Hingham, Mass., 1986.
- Fraedrich, K., Estimating the dimensions of weather and climate attractors, *J. Atmos. Sci.*, 43, 419-432, 1986.
- Gambis, D., Wavelet Transform Analysis of the Length of the Day and the El Niño/Southern Oscillation Variations at Intra-seasonal and Interannual Time Scales, *Ann. Geophys.*, 10, 429-437, 1992.
- Ghil, M., and K. Mo, Intraseasonal Oscillations in the Global Atmosphere, Part 1, Northern Hemisphere and Tropics, *J. Atmos. Sci.*, 48, 752-779, 1991.
- Ghil, M., and K. Mo, Intraseasonal Oscillations in the Global Atmosphere, Part 2, Southern Hemisphere, *J. Atmos. Sci.*, 48, 780-790, 1991.
- Ghil, M., and R. Vautard, Interdecadal oscillations and the warming trend in global temperature time series, *Nature*, 350, 324-327, 1991.
- Graham, N. E., J. Michaelson, and T. P. Barnett, An investigation of the El Niño-Southern Oscillation cycle with statistical models, 1, Predictor field characteristics, *J. Geophys. Res.*, 92, 14,251-14,270, 1987a.

- Graham, N. E., J. Michaelsen, and T. P. Barnett, An investigation of the ElNiño-Southern Oscillation cycle with statistical models, 2, Model Results, *J. Geophys. Res.*, 92, 14,271-14,289, 1987b.
- Gross, R. S., T. M. Eubanks, J. A. Steppe, A. P. Freedman, J. O. Dickey, and T. F. Runge, A Kalman filter-based approach to combining independent Earth orientation series, *J. Geodesy*, in press, 1997.
- Gross, R. S., Combinations of Earth Orientation Measurements—SPACE94, COMB94, and POLE94, *J. Geophys. Res.*, **101**, 8729-8740, 1996.
- Gross, R. S., S. L. Marcus, T. M. Eubanks, J. O. Dickey, and C. L. Keppenne, Detection of an ENSO Signal in Seasonal Length-of-Day Variations, *Geophys. Res. Lett.*, 23, 3373-3376, 1996.
- Hide, R., and J. O. Dickey, Earth's variable rotation, *Science*, 253, 629-637, 1991,
- Horel, J. D., and J. M. Wallace, Planetary-scale atmospheric phenomena associated with the Southern Oscillation, *Mon. Weather Rev.*, 109, 813-828, 1981.
- Jiang, N., J. D. Neeling, and M. Ghil, Quasi-Quadrennial and Quasi-Biennial Variability in the Equatorial Pacific, *Clim. Dyn.*, 12, 101-112, 1995.
- Jordi, C., L. V. Morrison, R. D. Rosen, D. A. Salstein, and G. Rosello, Fluctuations in the Earth's Rotation since 1830 from High-Resolution Astronomical Data, *Geophys. J. Int.*, **117**, 811-818, 1994.
- Keppenne, C. L., and M. Ghil, Adaptive filtering and prediction of the Southern Oscillation index, *J. Geophys. Res.*, 97, 20,449-20,454, 1992.
- Keppenne, C. L., and M. Ghil, Adaptive spectral analysis of the Southern Oscillation Index, in *Proceedings of the XVth Annual Climate Diagnostics Workshop*, pp. 30-24, U.S. Department of Commerce, NOAA, Springfield, VA., 1990.
- Keppenne, C. L. and M. Ghil, Extreme weather events, *Nature*, 358, 547, 1992.
- Lambeck, K., *The Earth's Variable Rotation*, Cambridge University Press, New York, 1980.

- Lambeck, K., and A. Cazenave, The Earth's rotation and atmospheric circulation, I, seasonal variations, *Geophys. J. R. Astron. Soc.*, 72, 79-93, 1973.
- Lau, K. M., and P. H. Chan, Aspects of the 40-50 day oscillation during the northern summer as inferred from outgoing longwave radiation, *Mon. Weather Rev.*, 114, 1354-1367, 1986.
- Mo, K. C., and M. Ghil, Interannual oscillations in the 700 mb geopotential height field over the northern hemisphere, *J. Clim.*, in press, 1992.
- Penland, C., M. Ghil, and K. M. Weickmann, Adaptive filtering and maximum entropy spectra, with application to changes in atmospheric angular momentum, *J. Geophys. Res.*, 96, 22,659-22,671, 1991.
- Pike, E. R., J. G. McWhirter, M. Gertero, and C. de Mel, Generalized information theory for inverse problems in signal processing, *IEEE Proc.*, 131, 660-667, 1984.
- Philander, S. G. H., El Niño Southern Oscillation phenomena, *Nature*, 302, 295-301, 1983.
- Rasmussen, E. U., and J. M. Wallace, Meteorological aspects of the El Niño/Southern oscillation, *Science*, 222, 1195-1202, 1983.
- Philander, S. G. H., El Niño, La Niña, and the Southern Oscillation, 293 pp., Academic, San Diego, Calif., 1990.
- Preisendorfer, R. W., *Principal Component Analysis in Meteorology and Oceanography*, edited by C. D. Mobley, 425 pp., Elsevier, New York, 1988.
- Press, W. H., B. P. Flannery, S. A. Teukolski, and W. T. Vetterling, *Numerical Recipes in C*, pp. 461-465, Cambridge University Press, New York, 1988.
- Rasmussen, E. M., and T. H. Carpenter, Variations in tropical sea surface temperature and surface wind fields associated with the Southern Oscillation/El Niño, *Mon. Weather Rev.*, 110, 354-384, 1982.
- Rasmussen, E. M., X. Wang, and C. F. Ropelewski, The biennial component of ENSO variability, *J. Mar. Syst.*, 1, 71-96, 1990.

- Rosen, R. D., D. A. Salstein, T. M. Eubanks, J. O. Dickey, and J. A. Steppe, An El Niño signal in atmospheric angular momentum and Earth rotation, *Science*, 22.5, 411-414, 1984.
- Rosen, R. D., The axial momentum balance of Earth and its fluid envelope, *Surv. Geophys.*, 14, 1-29, 1993.
- Salstein, D. A., and R. D. Rosen, Earth rotation as a proxy for interannual variability in atmospheric circulation, 1860-present, *J. Clim. Appl. Meteorol.*, 25, 1870-1877, 1986.
- Stephanie, M., Interannual atmospheric angular momentum variability 1963-1973 and the Southern Oscillation, *J. Geophys. Res.*, 87, 428-432, 1982.
- Trenberth, K. E., and D. J. Shea, On the Evolution of the Southern Oscillation, *Mon. Weather. Rev.*, **115**, 3078-3096, 1987.
- Vautard, R., and M. Ghil, Singular spectrum analysis in nonlinear dynamics, with applications to paleoclimatic time series, *Phys. D Amsterdam*, 35, 395-424, 1989.
- Vautard, R., P. Yiou, and M. Ghil, Singular spectrum analysis: A toolkit for short, noisy chaotic signals, *Phys. D Amsterdam*, 58, 95-126, 1992.
- Walker, G., On periodicity in series of related terms, *Proc. R. Soc. London, Ser. A*, 131, 518-532, 1931.
- Weare, B. C., and J. S. Nasstrom, Examples of extended empirical orthogonal function analyses, *Mon. Weather Rev.*, 110, 481-485, 1982.
- Wyrski, K., Water displacements in the Pacific and the genesis of El Niño cycles, *J. Geophys. Res.*, 90, 7129-7132, 1985.
- Xu, J. S., On the Relationship Between the Stratospheric Quasi-Biennial Oscillation and the Tropospheric Southern Oscillation, *J. Atmos. Sci.*, 49, 725-734, 1992.
- Yule, G. U., On a method of investigating periodicities in disturbed series, *Philos. Trans. R. Soc. London, Ser. A*, 226, 267-298, 1927.

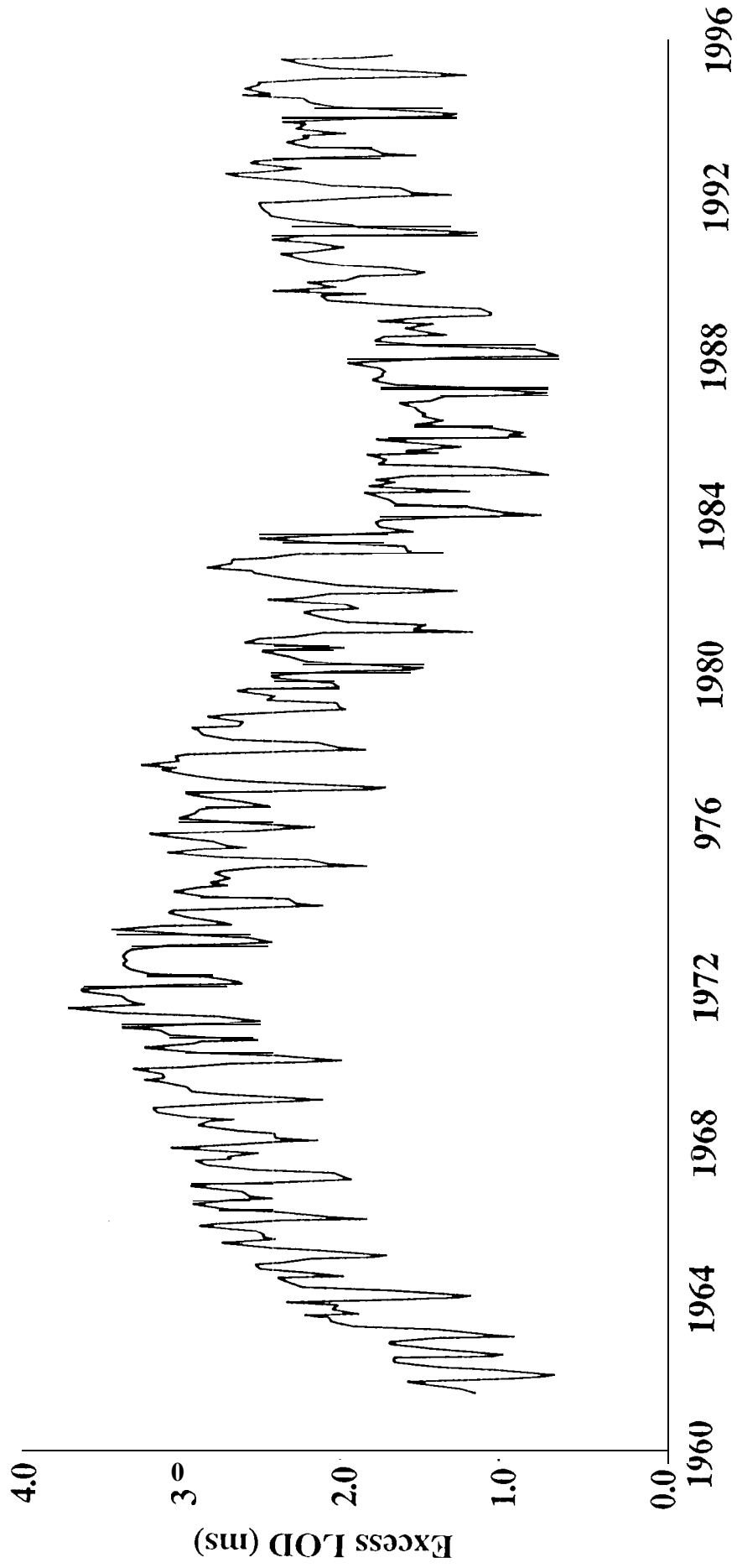


Fig 1

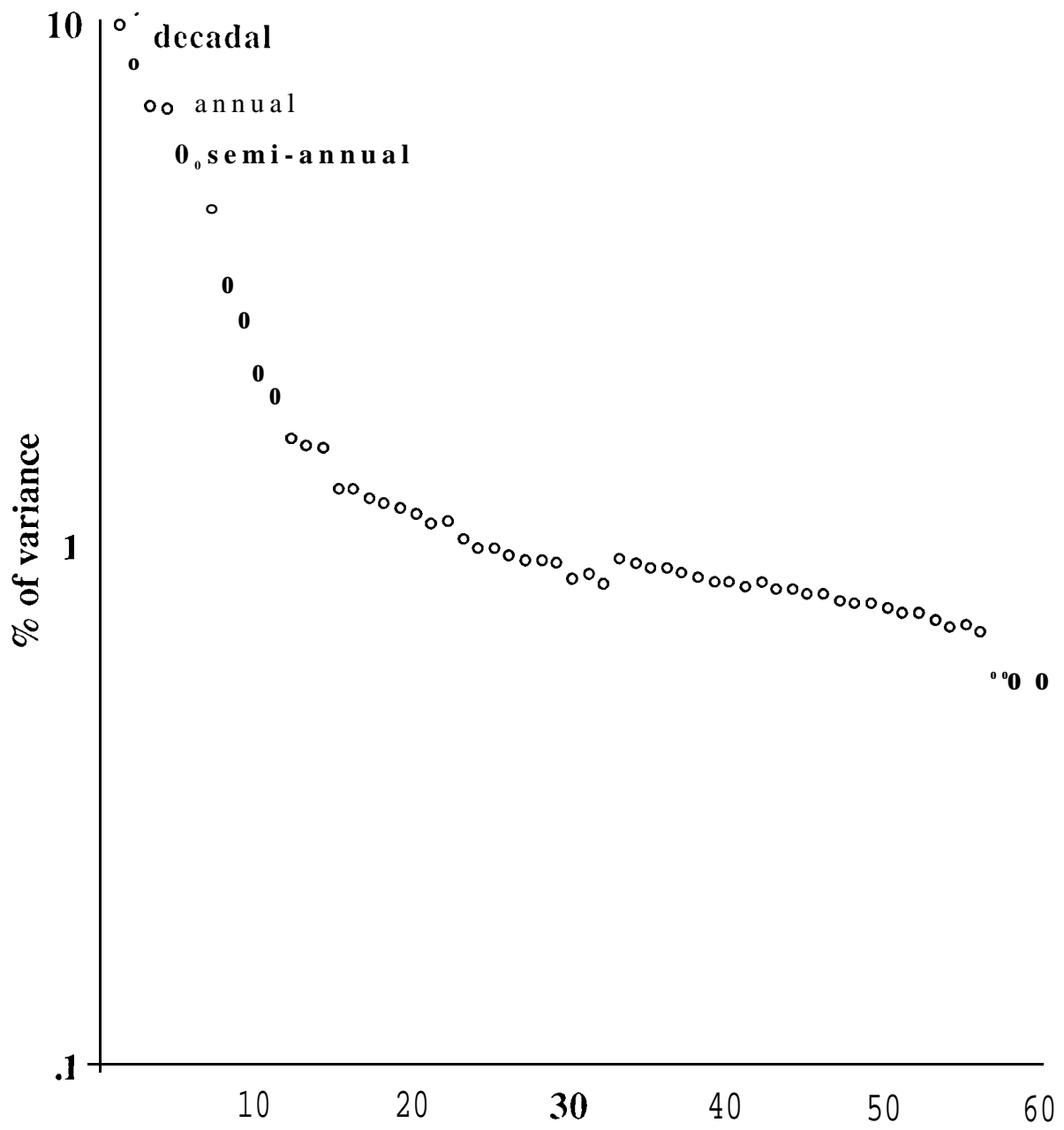


Fig 2

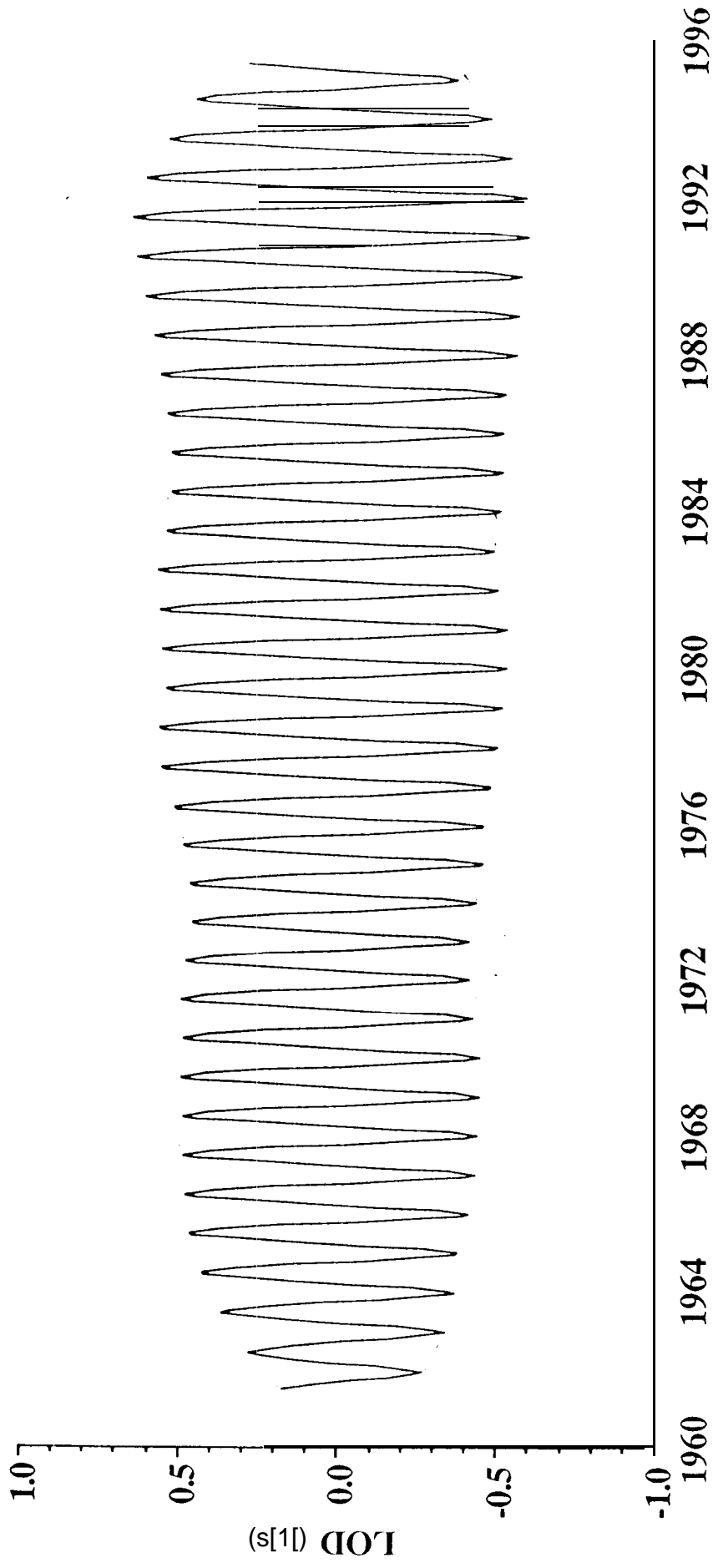
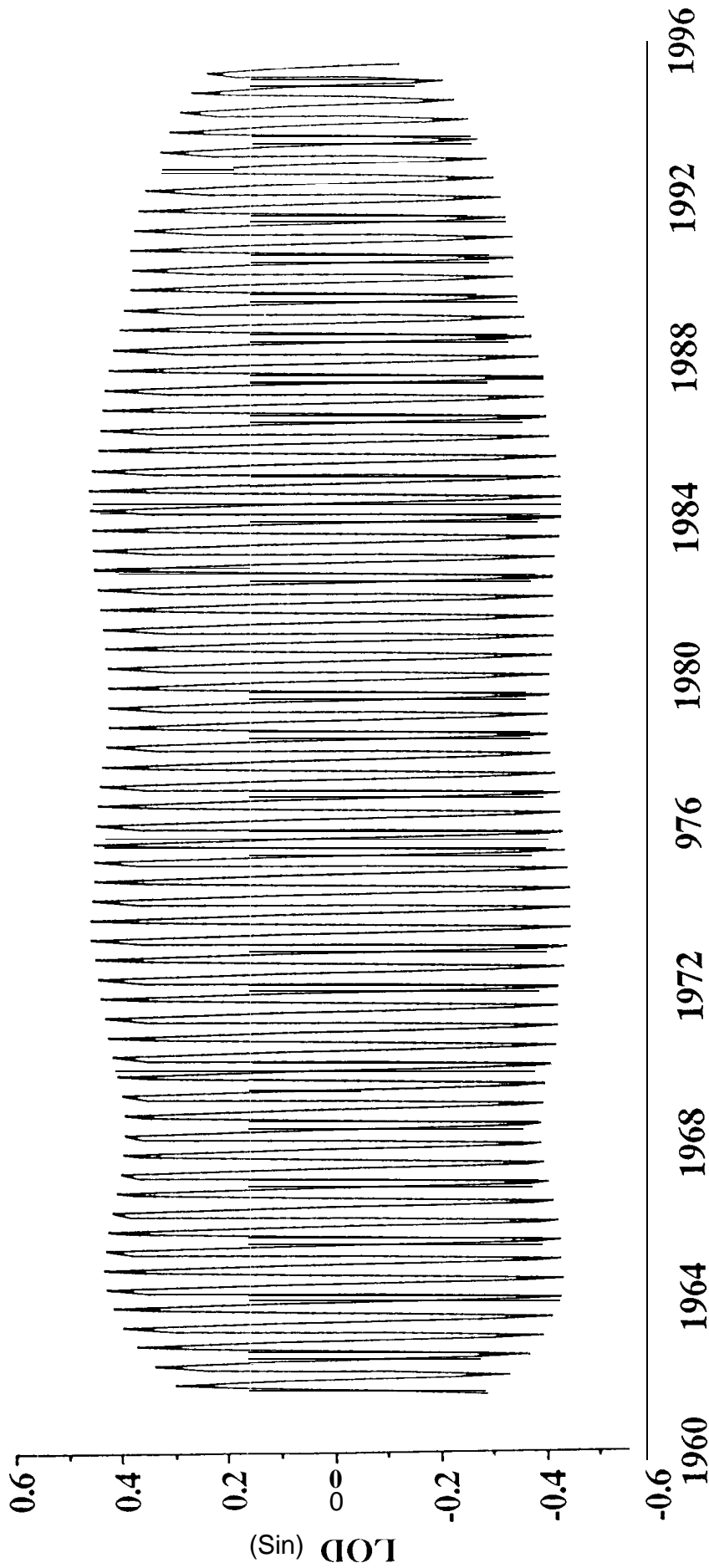


Fig 3a



*Fig 36*

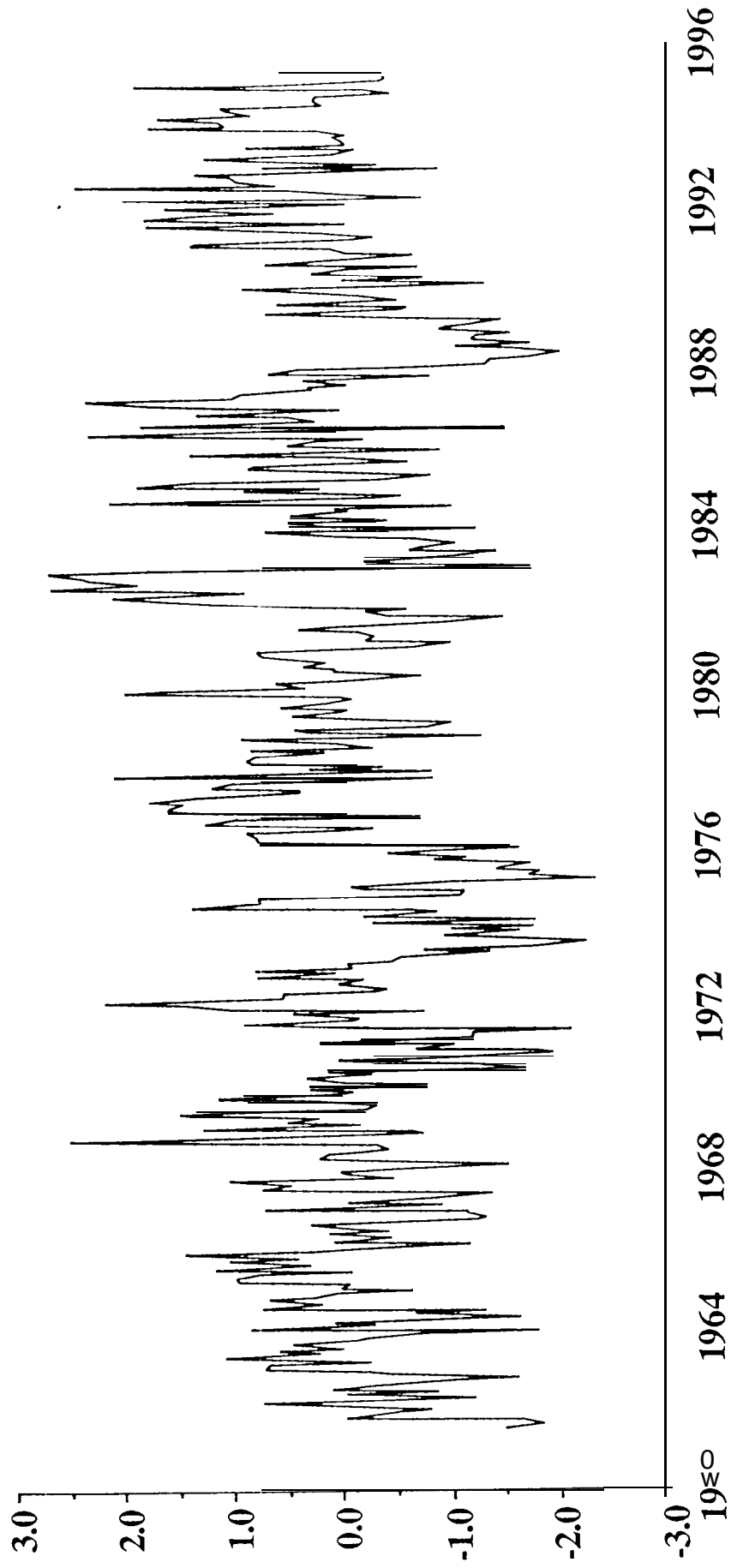


Fig 4a

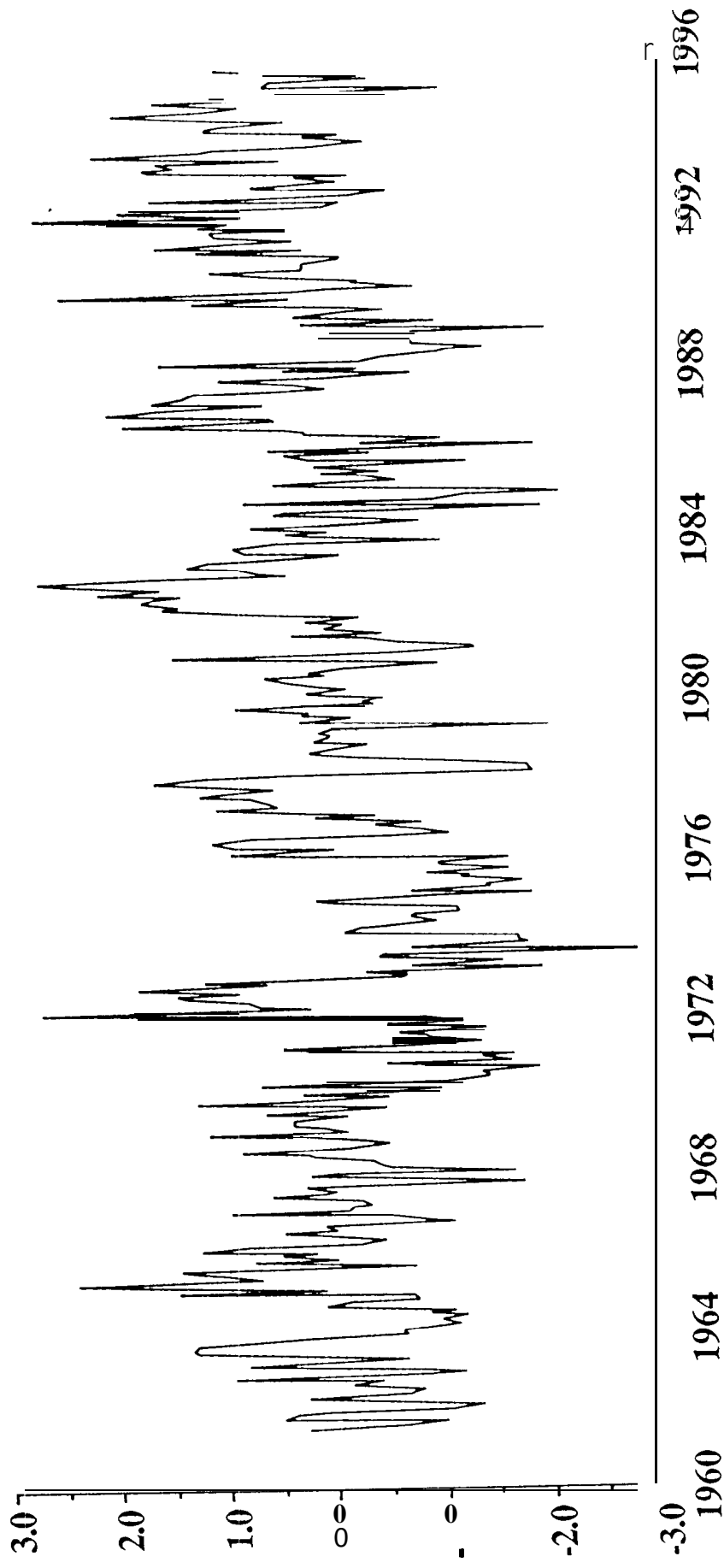


Fig 40

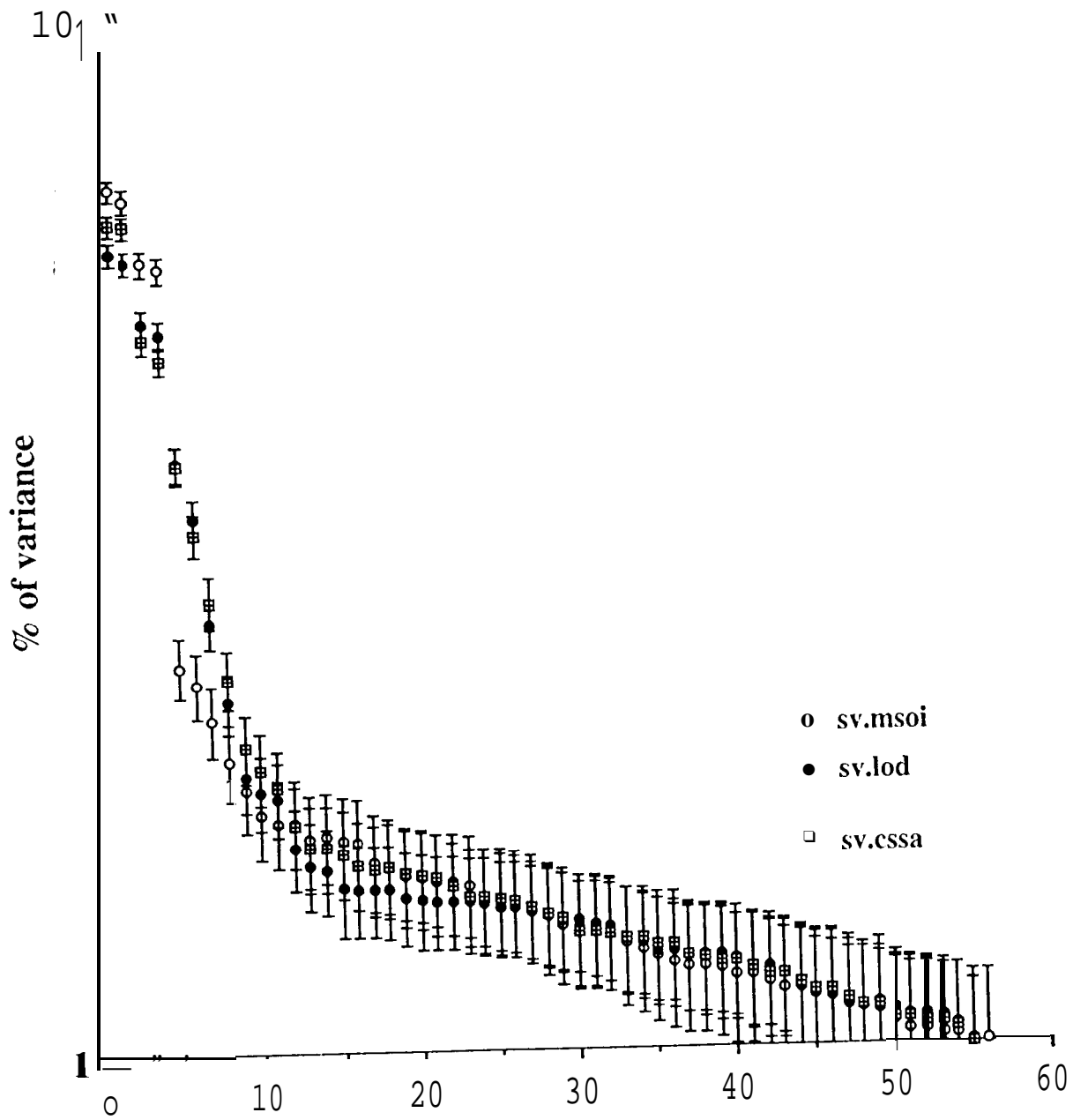


Fig 5

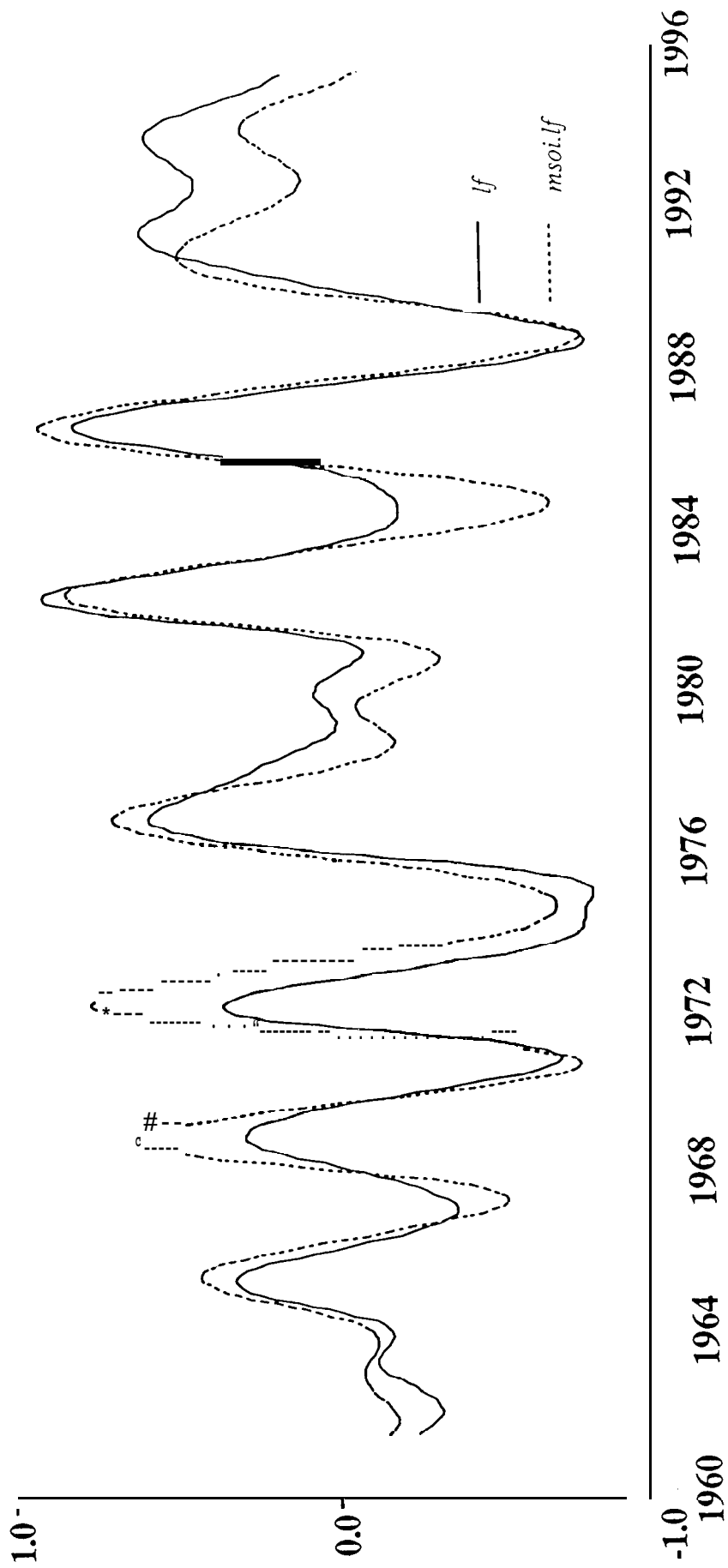
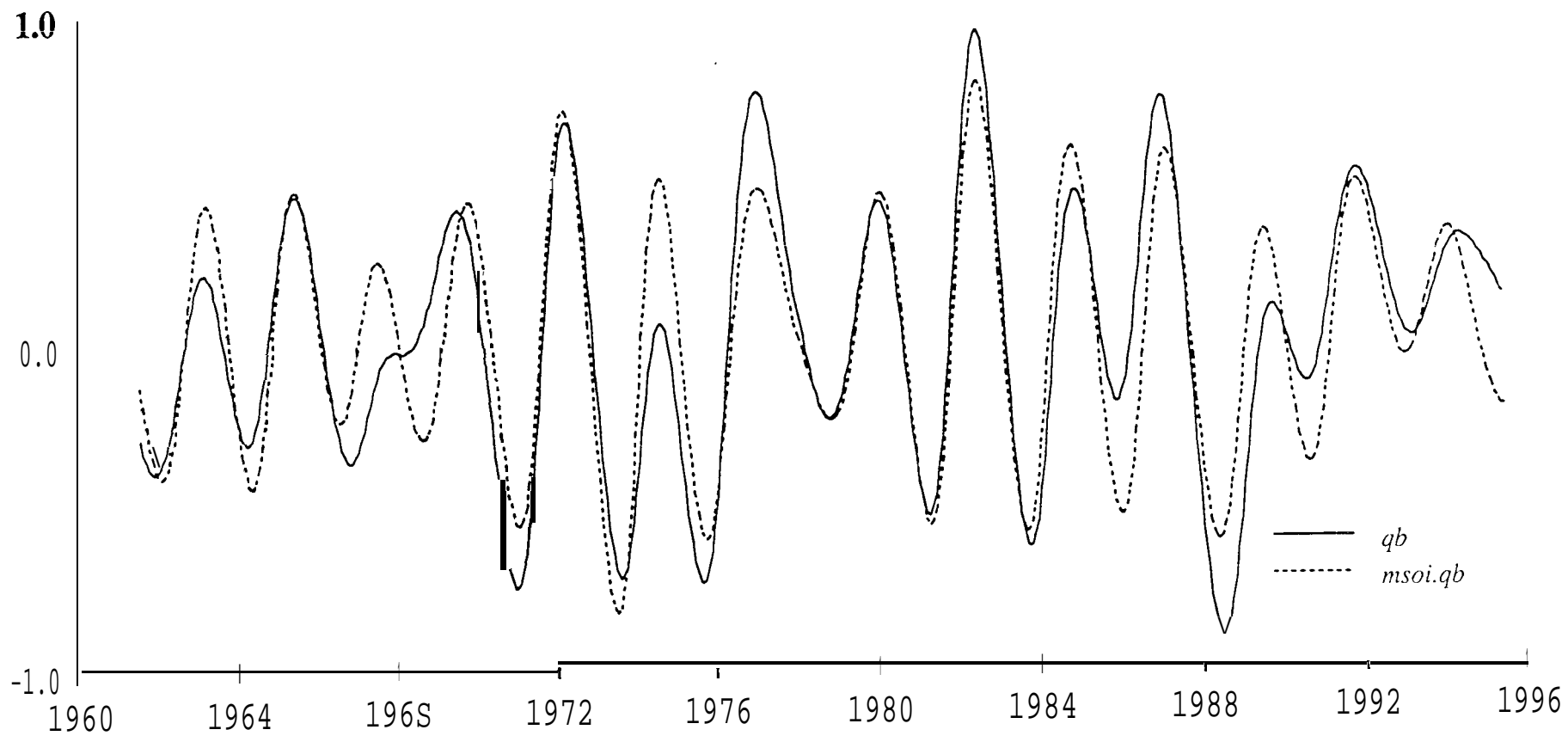


Fig 2



*F, 11/02*

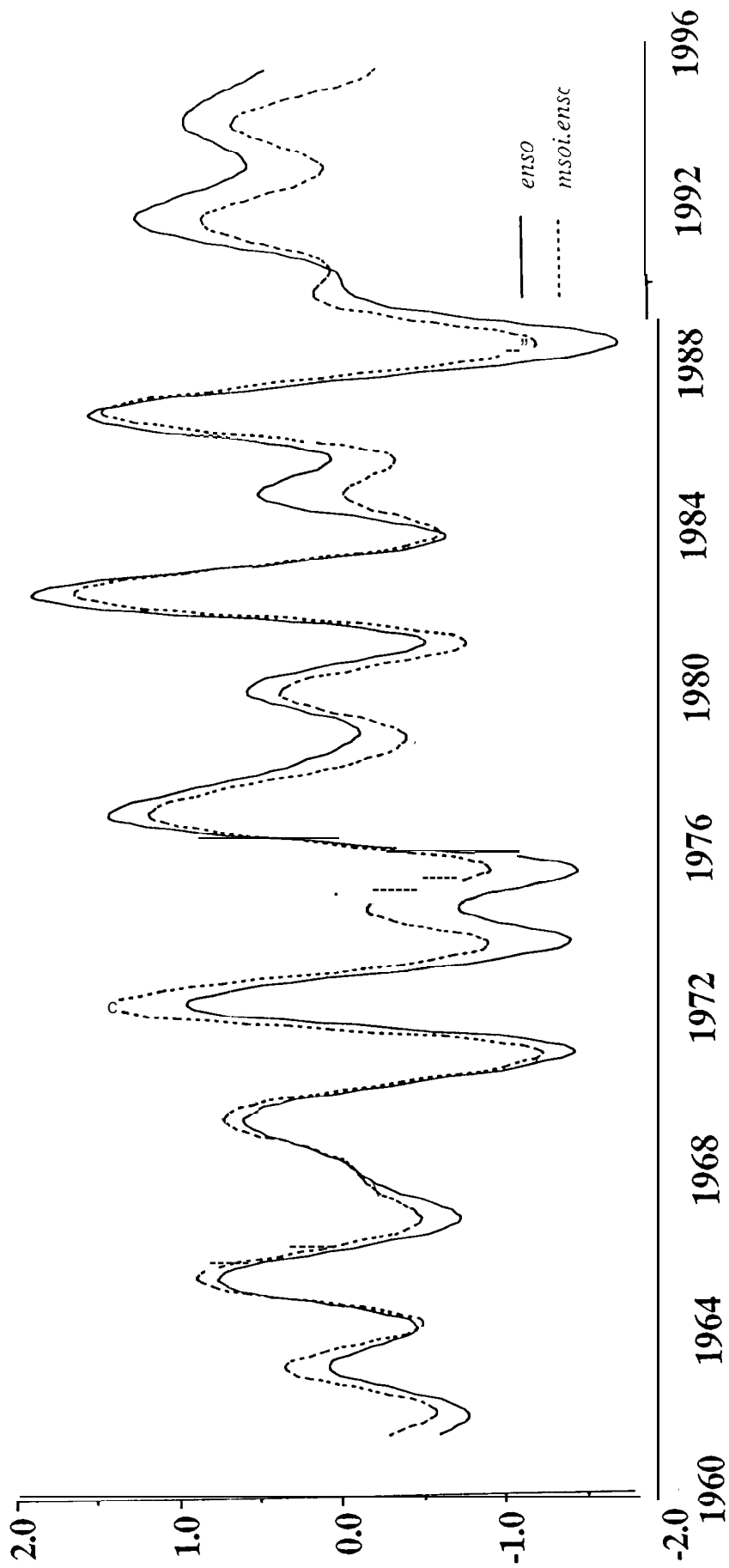
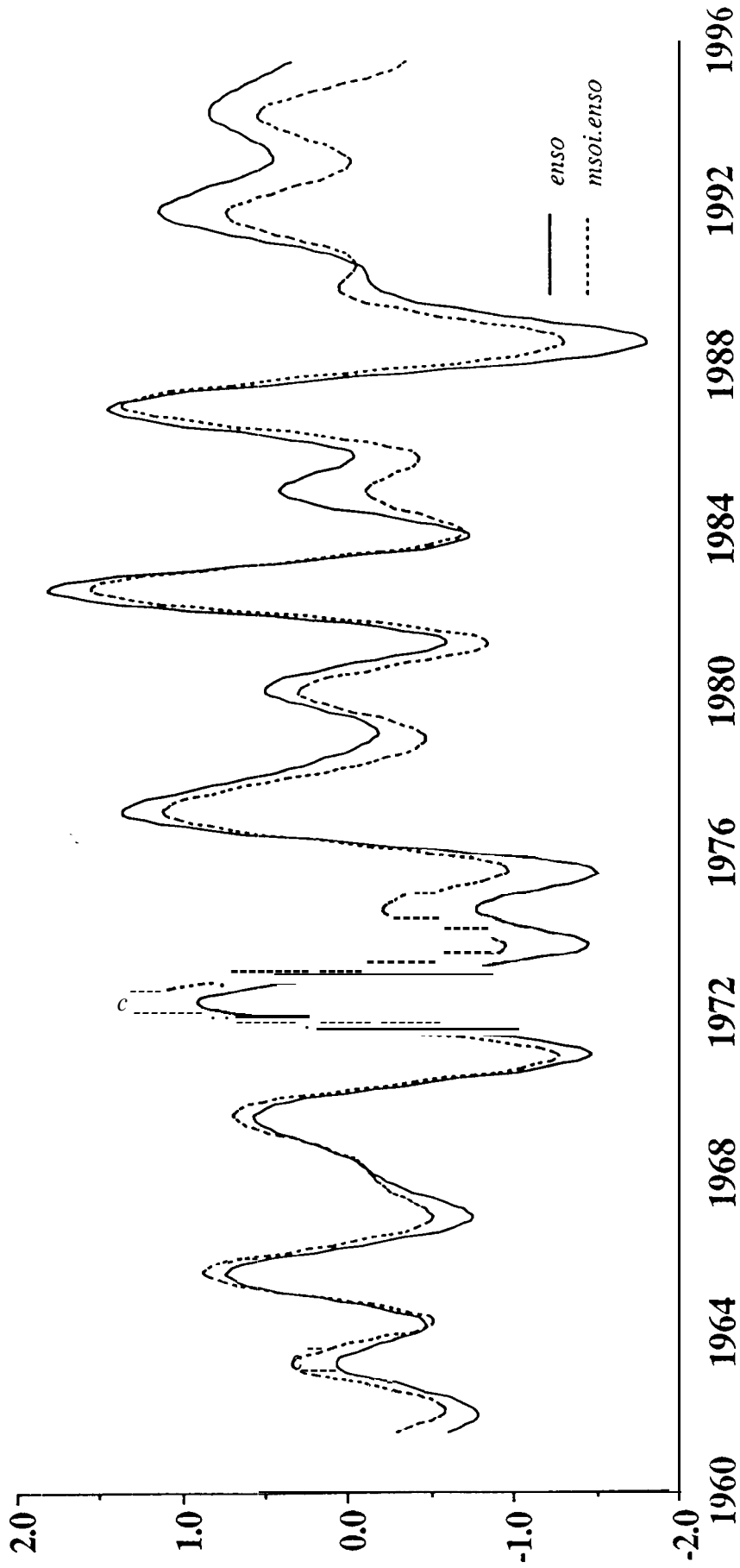


Fig c



62

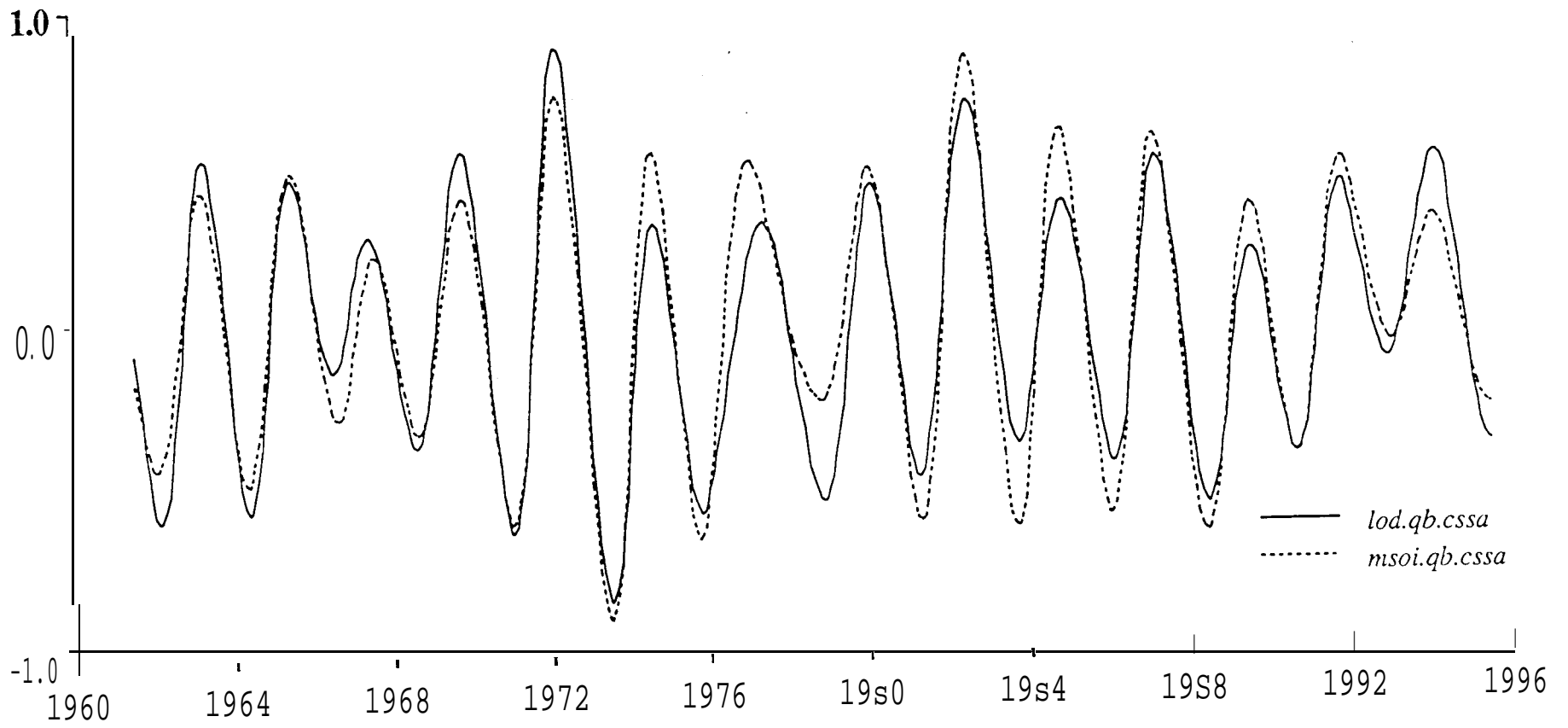
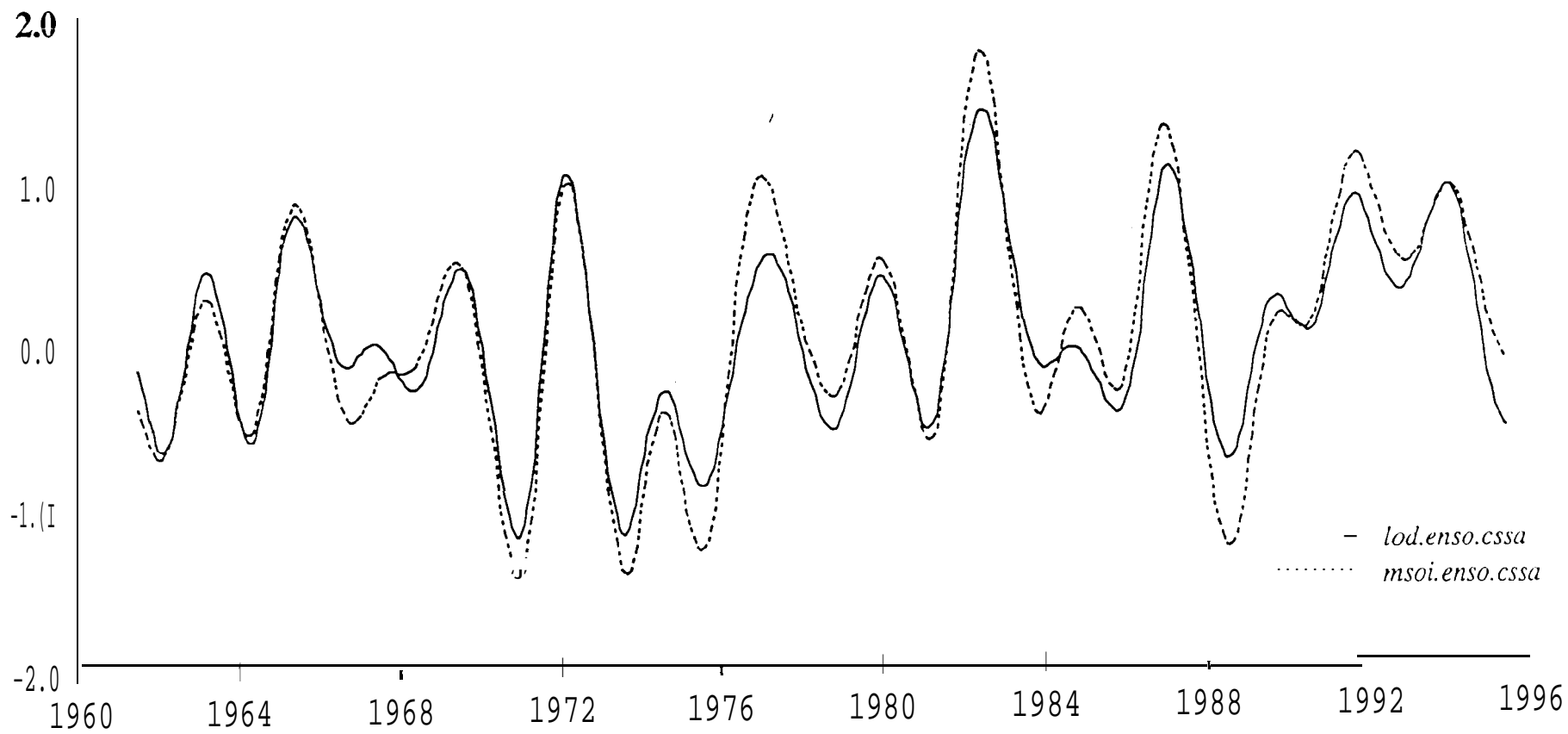


Fig 6e



*Fig 6f*

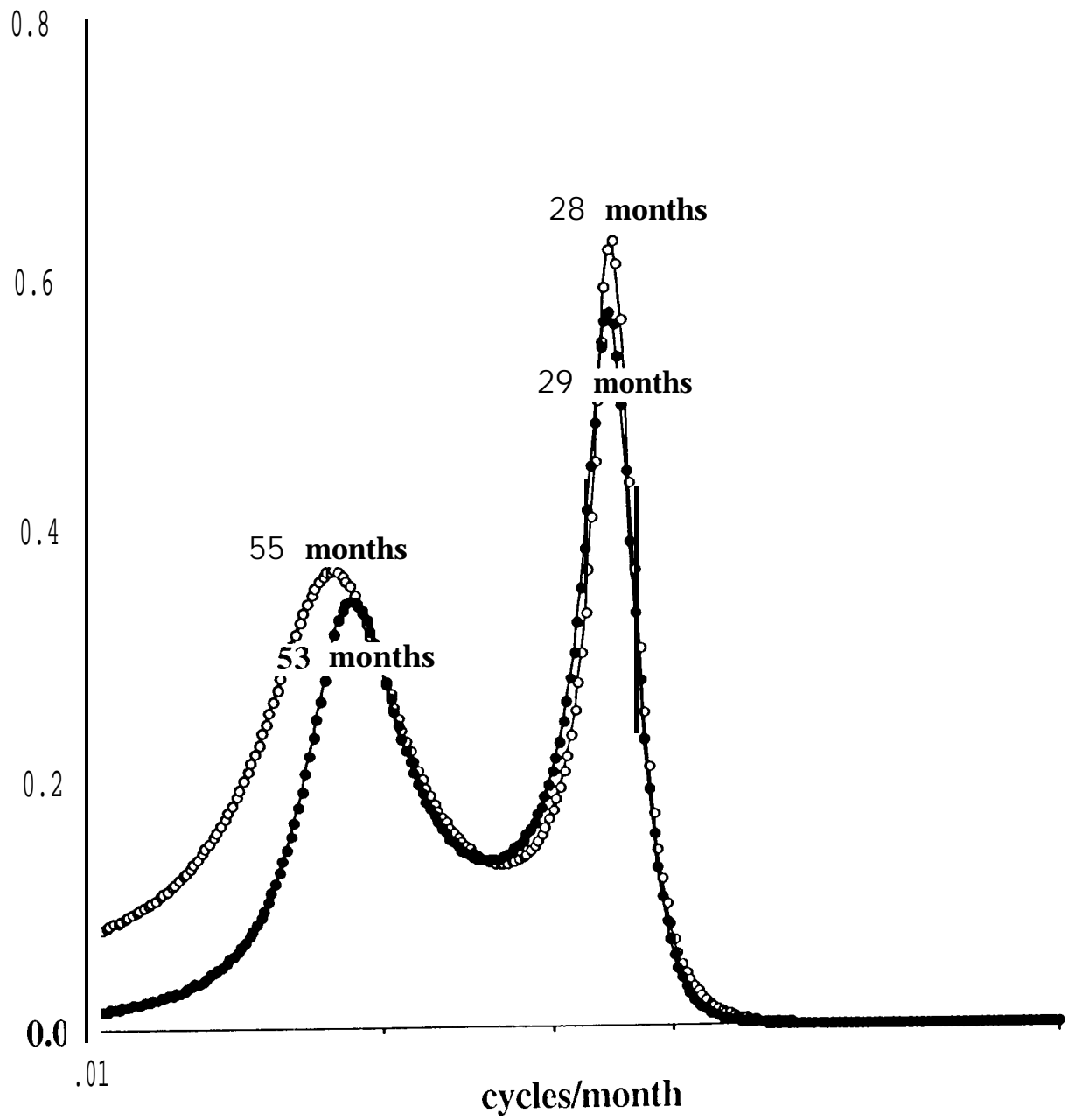
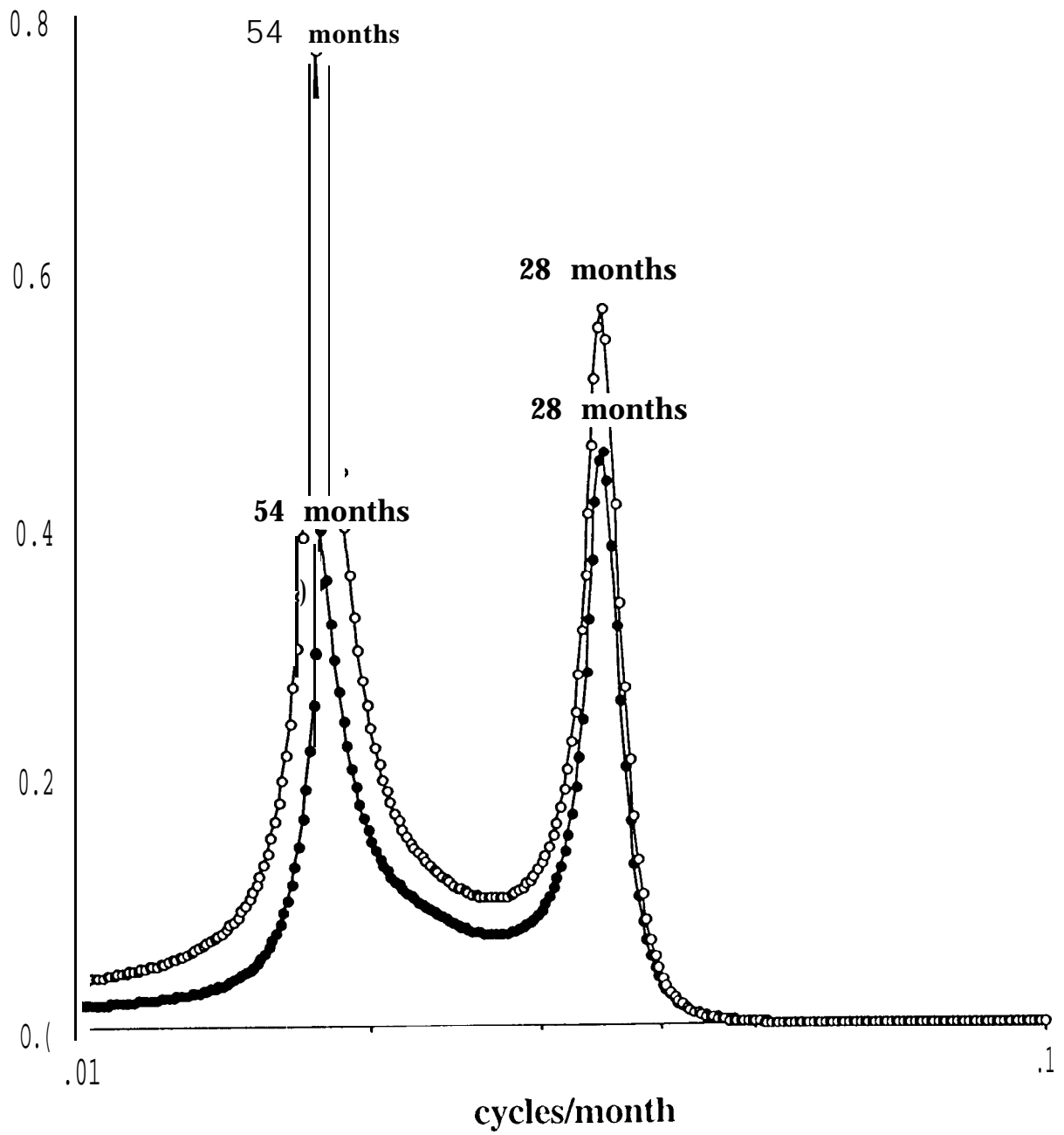
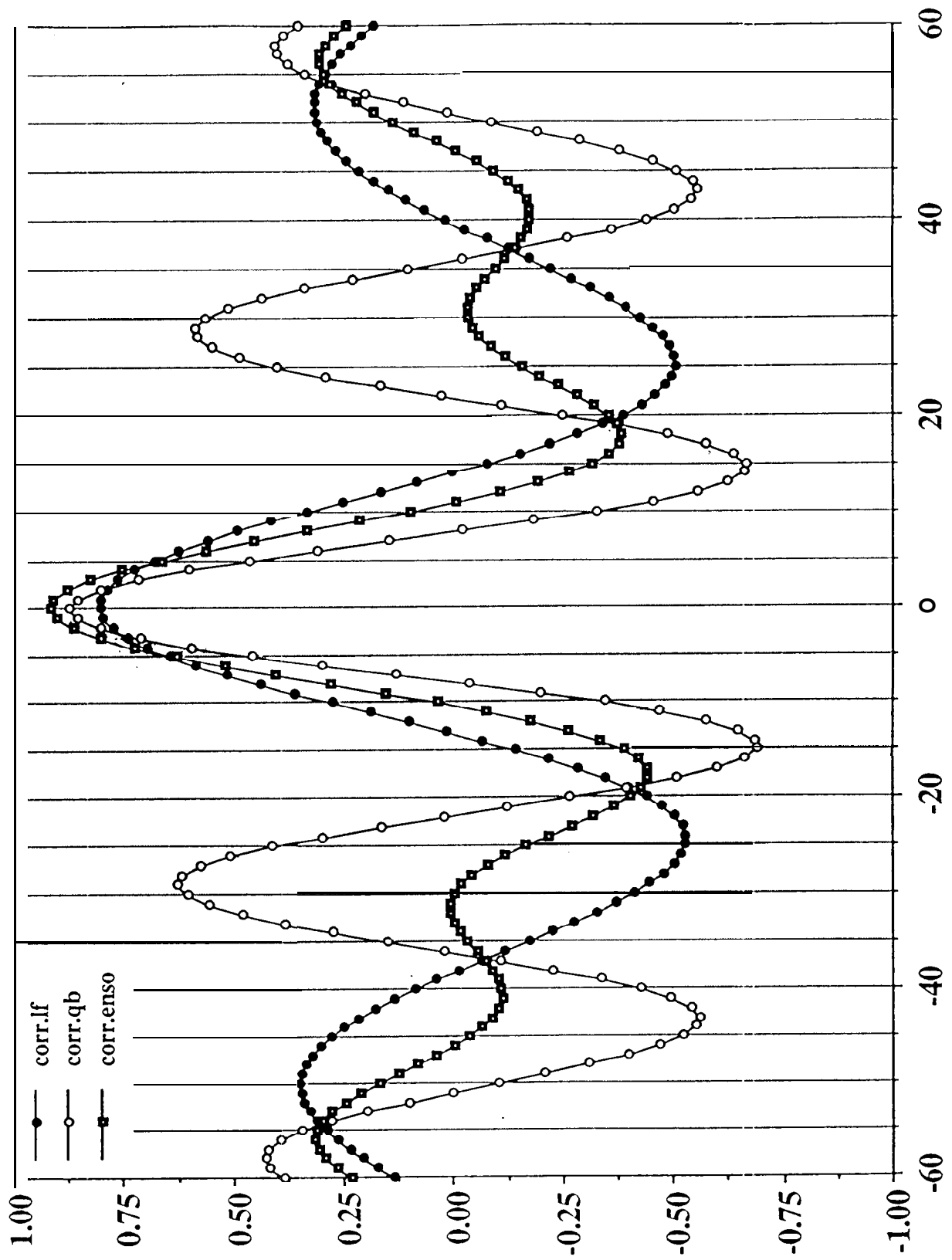
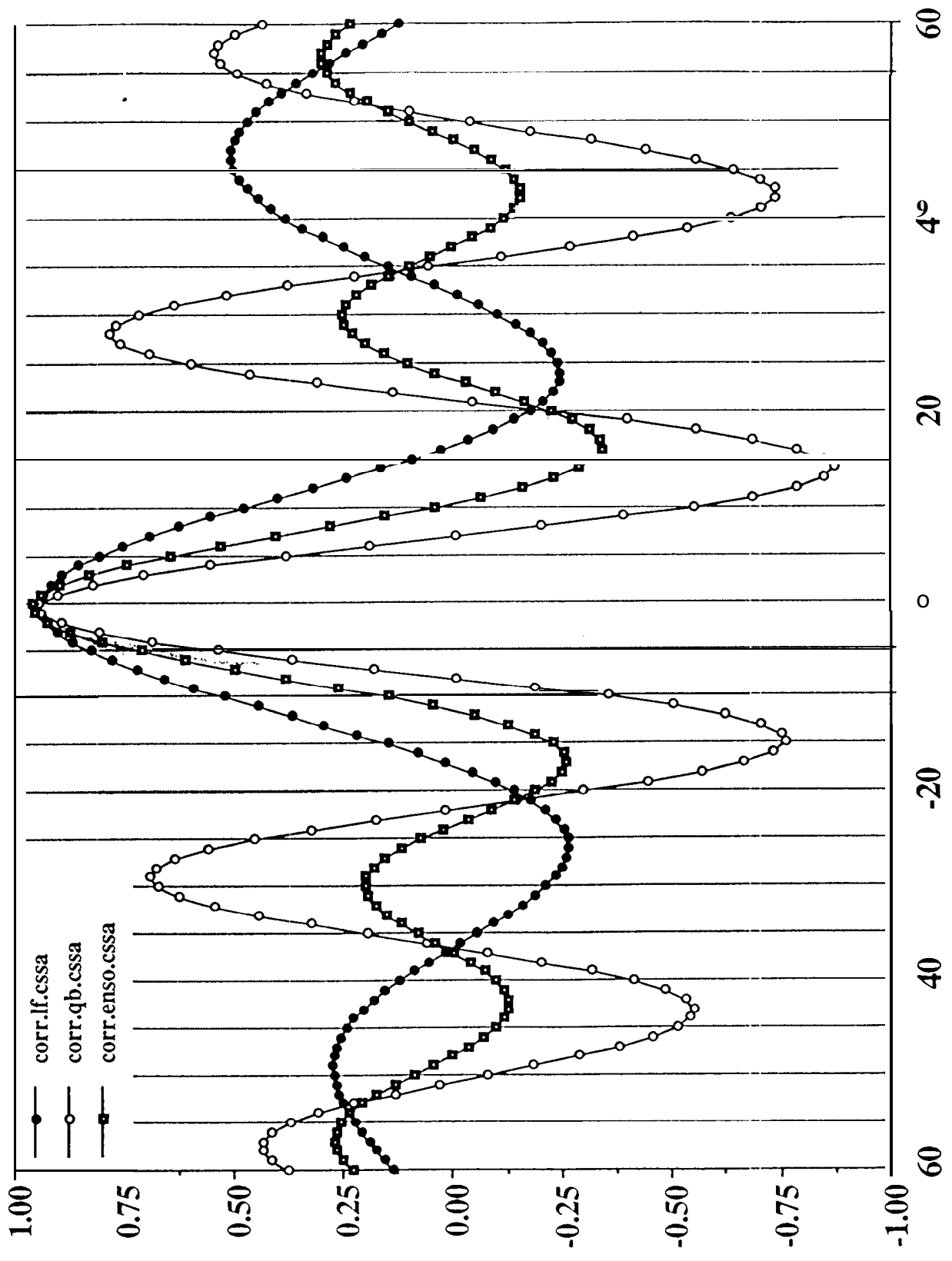


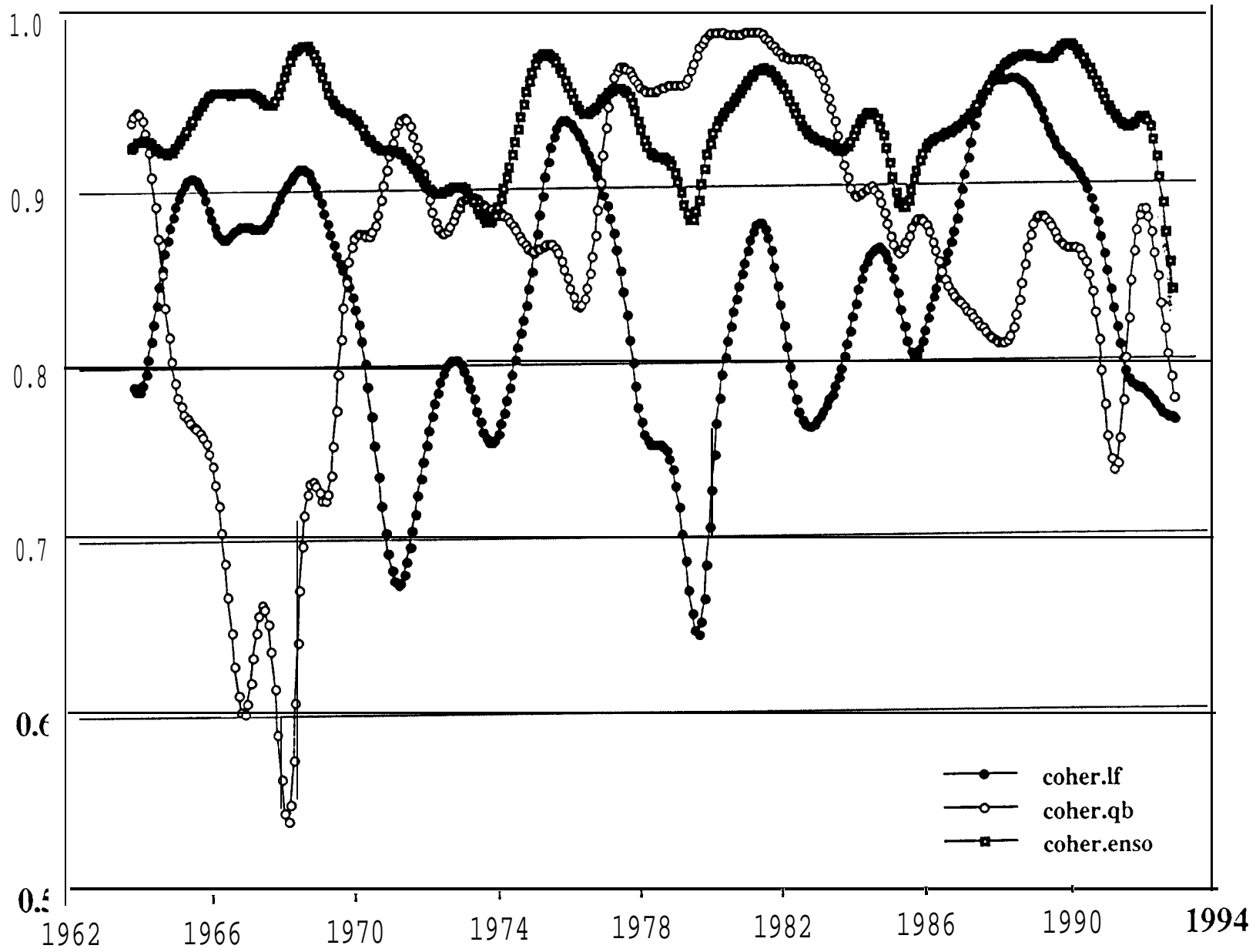
Fig 7a





8a,





90 90

